



# Hybrid framework for respiratory lung diseases detection based on classical CNN and quantum classifiers from chest X-rays

G.V. Eswara Rao <sup>a</sup>, Rajitha B. <sup>a</sup>, Parvathaneni Naga Srinivasu <sup>b,c</sup>, Muhammad Fazal Ijaz <sup>d,\*</sup>, Marcin Woźniak <sup>e,\*</sup>

<sup>a</sup> CSED, Motilal Nehru National Institute of Technology Allahabad, Prayagraj, 211004, Uttar Pradesh, India

<sup>b</sup> Department of Computer Science and Engineering, Prasad V Poturi Siddhartha Institute of Technology, Vijayawada, 520007, Andhra Pradesh, India

<sup>c</sup> Biomedical Data Analytics Research Group, Department of Teleinformatics Engineering, Federal University of Ceará, Brazil

<sup>d</sup> School of IT and Engineering, Melbourne Institute of Technology, Melbourne, 3000, Australia

<sup>e</sup> Faculty of Applied Mathematics, Silesian University of Technology, Kaszubska 23, Gliwice, 44100, Poland



## ARTICLE INFO

### Keywords:

Convolutional neural network  
Feature extraction  
Quantum machine learning  
Quantum classifier  
Qubits

## ABSTRACT

The human respiratory system might be seriously affected by COVID-19 infection. Therefore, early classification of it is a crucial task. Quantum machine learning and quantum neural network models can play an effective role in multiclass classification problems. Compared to standard deep and machine learning classifiers, the quantum variational classifier may lead to less memory usage, accuracy, and portability for respiratory disease detection. This article proposes a hybrid respiratory lung disease detection framework based on classical CNN and Quantum classifiers. It combines a classical deep feature extraction model with quantum classifiers. A new custom convolutional neural network (CCNN) deep learning model is proposed to perform feature extraction, and the Multi-Multi-Single (MMS) & Multi-Single-Multi-Single (MSMS) are proposed as quantum machine learning algorithms. These two quantum classifiers are built via a quantum variational circuit with encoding, entanglement, and measurement properties. The tests were carried out on the COVID-19 Radiography Dataset (CRD), which contains 15,153 chest X-ray images of COVID-19, Viral, and Normal. The experimental results revealed that the proposed model had the highest training and testing accuracy of 98.9% and 98.1%, on the CRD dataset, with a computation cost of 0.07 and 0.08 respectively. This hybrid model performs better than the other standard deep learning models. Additionally, we validated our MMS and MSMS quantum classifiers by deploying them on the IBM Q-QASM real-time quantum computer.

## 1. Introduction

Detecting and classifying respiratory diseases and their severity is essential for monitoring their spread, analyzing their features, and developing effective public health treatment. There are many different respiratory diseases, and researchers have classified them into three broad categories: variants of interest, variants of concern, and variants being monitored. These acute respiratory diseases are viral, pneumonia, and Coronavirus (COVID-19); their variations are delta, alpha, gamma, and beta. The global pandemic was brought on by COVID-19, produced by severe acute respiratory syndrome coronavirus 2 (SARS-CoV-2) [1,2]. In Wuhan, Hubei Province, China, there were 27 pneumonia patients at the center of the initial outbreak in late 2019. On March 11, 2020, the virus was first deemed a pandemic due to its quick global spread [3,4]. The World Health Organization (WHO) has declared a pandemic COVID-19. COVID-19 symptoms include high fever, tiredness, coughing, loss of taste, and breathing problems. In severe cases,

the virus causes pneumonia. Thus, the body loses oxygen. The patient's symptoms develop 6–7 days after COVID-19 grows, which takes 3–13 days. The WHO has reported 396,558,014 COVID-19 cases worldwide, with 5,745,032 deaths. A severe acute respiratory syndrome-related infectious disease is COVID-19. The COVID-19 virus's features and variations make it extremely challenging to identify patients earlier. The severity of lung-based diseases can be determined through various medical tests.

During the COVID-19 pandemic, different validation approaches [5–7], applications, and hardware tools have been presented based on the symptoms, such as Reverse transcription polymerase chain reaction (RT-PCR), chest X-ray (CXR), computed tomography (CT), Thermal imaging, etc. Chest X-ray imaging can be applied to quickly and effectively identify the problem. Since they might present respiratory issues even at an advanced stage of COVID, viral, and other lung diseases. Deep Learning (DL) and Machine Learning (ML) algorithms have been

\* Corresponding authors.

E-mail addresses: [mfazal@mit.edu.au](mailto:mfazal@mit.edu.au) (M.F. Ijaz), [marcin.wozniak@polsl.pl](mailto:marcin.wozniak@polsl.pl) (M. Woźniak).

developed in recent years to enhance the detection and classification of diseases. This paper presents a hybrid classical CNN and Quantum Classifier(QC) network for detecting and classifying respiratory diseases. The results confirmed that the proposed strategy for detecting and classifying respiratory diseases is effective. Two quantum-based classifiers are used to train the proposed hybrid classical CNN and quantum-based classifier. The results show that the proposed method can accurately detect and classify respiratory diseases.

### 1.1. Deep learning approaches

Deep learning is a highly effective mechanism with the potential to collect information, process information, and then provide the users with an adequately specified output. In contrast with traditional or manual feature extraction approaches, this minimizes time and costs. Adopting artificial intelligence (AI) in acute respiratory distress syndrome (ARDS) opens up a wide range of respiratory disease classification methods. Deep convolutional networks and recurrent neural networks(DCNN) [8], mainly two Deep Learning approaches, are now the basis upon which AI technologies have achieved this primary scope. In terms of providing more output feature maps, these models have a lot of potential to be applied to the classification of chest X-ray images. Likewise, DL-based models such as V-Net and ResNet have been explored for improving image segmentation to identify risky lesions. Also, Deep convolutional neural network (DCNN) models were used to extract features. These models are constantly being examined in various domains that assess the intensity of respiratory disease in human ARDS. It has been trained to automatically detect the expected number of cases using a dataset from all major global cities. Deep learning approaches aim to develop a reliable respiratory disease prediction tool. Deep learning techniques are capable of classification and segmenting images. Despite these deep learning benefits, training becomes more complex and costly when assessing large image datasets. It demands more expensive computing systems.

### 1.2. Quantum mechanics-based approaches

Quantum machine learning, on the other hand, is a new form of technology that really can provide more cost-saving solutions. Scientists have achieved significant remarkable progress owing to quantum machine learning [9–11]. On the other hand, it has been proven that the Quantum Neural Network (QNN) field can solve complex challenges with classical computers [12–14]. Researchers reported a variety of quantum transfer learning methods based on the QNN model to overcome the classification problems, as well as in terms of network training and classification. These hybrid systems define the nature of the network, which combines classical and quantum modules. The objective of the quantum transfer learning method is to minimize starting from scratch and instead rely on already acquired skills. Three versions of the standard transfer learning methods [15] have so far been advanced: the Classical–Quantum (CQ), Quantum–Classical (QC), and Quantum–Quantum (QQ) methods.

### 1.3. Need of hybrid quantum mechanics

The architecture parameters for the conventional approaches up to now are very high. Therefore, it might not be compatible with mobile devices with less Memory space. Thus, quantum-based models can solve this problem by minimizing the storage requirements. As an outcome, the overall hyperparameter performance of QC, CQ, and QQ can be optimized [16–18]. Using a hybrid classical–quantum approach [19–23], this study uses chest X-ray images to classify COVID-19 from other respiratory diseases. For classification of respiratory disease in this context, the quantum circuit [24] is designed and trained on its deep learning model. This research aims to combine feature selection using a classical network with quantum circuit classifying of chest X-ray images. The primary objective is to improve performance and use limited resources while promptly detecting various respiratory diseases.

### 1.4. Challenges in proposed approach

**Following are the challenges faced while designing the model:**

- One of the biggest challenges in defining the hybrid CCNN and Quantum classifier-based model architecture is building and configuring the feature extraction model and quantum circuit classifier.
- Implementing quantum circuits on real-time quantum processors is challenging because of their limited qubit size.
- Quantum devices have severe noise restrictions during the pre-processing of high-resolution images.
- The quantum circuit's depth may influence the performance of hybrid-based transfer models.

### 1.5. Contributions of proposed approach

**The following are the contributions made concerning the proposed approach:**

1. The major challenge of classical neural networks is that they have a large number of trainable parameters and thus consume more power. Hence, this proposed model is targeted for reduction in terms of size and cost.
2. Here, classical trainable parameters are optimized via encoding qubits, generating entangled quantum states, measuring the output of classical computers, and increasing the number of qubits.
3. To highlight the effectiveness of the proposed models (MMS and MSMS), we compared them to other machine learning models and a variety of classical models [25], including Mobile Net and Visual Geometry Group. (VGG16), Inception Net, ResNet50.
4. An improved custom CNN Quantum–classical model is also tested and evaluated using a real quantum processor, IBMQ-QASM. Where in the model is it proven capable of handling the noisy limitations on the extracted features of high-resolution images (explained in detail under sections).
5. In the conclusion, it was found that the experiment's results were satisfactory and exceeded previous models in terms of qubits, qdepth, training and testing accuracies, precision, sensitivity, false positive rate (FPR), F1-Score, Area Under Curve(AUC) and model size.

The later sections of this paper were organized as follows:

Description of existing deep learning, quantum transfer learning models, and Key concepts are given in Section 2. Section 3 discusses the architecture of the proposed feature extraction methods and quantum classifiers in detail. Section 4 illustrates the experimental setup and dataset used. Section 5 thoroughly analyzes the proposed model's comparative performance. Section 6 addresses the conclusion and future discussion.

## 2. Related work

In this section, we present multiple studies that use CNNs and quantum-based approaches to classify respiratory diseases.

### 2.1. Hybrid classical and quantum–classical transfer learning models

This hybrid quantum transfer approach aims to improve classical models by substituting quantum circuits for classical classifiers. The model first starts with a new proposed classical network to prepare the features from the provided dataset. Second, the reduced classical input features are transformed into quantum states, and the quantum state values are then performed on the proposed quantum circuit. The desired qubits are then measured for respective classical output values.

The measured classical values are also trained on a classical computer for additional multi-label classification.

In 2021, Jamil and Rahman [26] proposed a dual-stage-based DL method in this study to precisely recognize the presence of COVID-19 and its variations using CT scans and chest X-ray images. Deep convolutional models were then utilized to extract spatial features, while handcrafted features were extracted from a range of handcrafted descriptors. Initially, a convolutional neural network was used for detection. Ullah et al. [27] proposed a DL-based classification scheme for the SARS-CoV-2 Omicron subtype in 2022. This model uses a temporal CNN in a neural network to reliably identify the different COVID-19 strains. To distinguish COVID-19 variations, a temporal convolution network was utilized to capture feature sequences.

Showkat and Qureshi [28] propose the usage of DL in 2022 to address complex CXR image classification problems; DL is a network built using large datasets for an objective-like classification. Transfer Learning (TL) generates feature representations when there aren't enough datasets. Essam et al. [29] proposed the hybrid quantum-classical model for detecting different respiratory diseases, which include COVID-19, pneumonia, and normal. Traditional machine learning models that use chest X-rays do better than this one. It has an accuracy of 88.6% for binary classification and 99.6% for multi-class classification. So, a quantum-based classifier can also be used for categorizing COVID-19 data.

Araf et al. [30] suggested the SARS-CoV2 Omicron variant for genetics, transmission, and COVID-19 vaccine reactions. Mutations caused by SARS created several new types of CoV-2. Due to the new Omicron variant, there is a lot of sickness. To stop the impending outbreak, research was done on the SARS-CoV-2 Omicron variant to determine if it was contagious, how common it was, and how severe it was. Andrea Mari et al. [19] suggested a classical to quantum transfer learning model on Hymenoptera to classify images of ants and bees. This model uses ResNet18 to extract features [31,32], which are then processed to a 4-quantum bit circuit for subsequent binary classification. This model is evaluated with 1024 iterations on two distinct quantum processors. Their predictions are 97% accurate.

Andrea Mari et al. [19] developed a novel CQ transfer technique on the CIFAR-10 dataset for multiclass classification. This technique extracted features with ResNet18, and 512 features were extracted. Then, a distinct trainable quantum circuit was proposed with various parameters. The results indicate that the highest accuracy of the models is 97.6%. Hence, the respiratory diseases classification process might also be deployed to a quantum-based classifier.

## 2.2. Preliminaries

This section focused on a few essential quantum computing notations that can help readers to understand the terminology used in this discipline.

### 2.2.1. Mathematical background of quantum computing

Quantum computers handle classification problems based on quantum mechanics, such as quantum bits, superposition, and entanglement. Binary digits, such as 0s and 1s, are classical computers' primary data storage units. They are referred to as bits. The represented bits can come from complex data structures like audio or image pixels. However, a quantum computer stores data using the smallest unit possible, known as quantum bits (Qubit) [33]. A qubit can have a value of 0 or 1 at any given time, or both values simultaneously. Quantum mechanics only allows us to estimate the probability that an electron has a +1/2 or -1/2 spin at any given time. This requires the particles to spin in parallel, a phenomenon known as Entanglement [34]. Two classical bits are now equal to one qubit, and one qubit is now equal to two classical bits. Furthermore,  $N$  qubit is the same as  $2^n$  classical bits. A quantum gate often operates these Qubits, or unitary transformation matrix. This unitary matrix must meet the requirements of  $UU^\dagger = I \Rightarrow U^{-1} = U^\dagger$  [35]. We require the following basic states to build the unitary operators:

### 2.2.2. Quantum bits

In a quantum computer, the  $|0\rangle$  or  $|1\rangle$  symbols denote the basis state of a single qubit (Eq. (1)). This is the way Dirac notation is usually expressed (Bra-Ket). Below is a representation of the linear matrix of these states:

$$|0\rangle = \begin{pmatrix} 1 \\ 0 \end{pmatrix}, \quad |1\rangle = \begin{pmatrix} 0 \\ 1 \end{pmatrix} \quad (1)$$

Eq. (2) depicts the following for the linear combination of the  $|0\rangle$  and  $|1\rangle$  complex basis states in Hilbert space [36].

$$|\varphi\rangle = \alpha|0\rangle + \beta|1\rangle \quad (2)$$

If a quantum operation is done on a qubit in more than one state, the operation is done on all states simultaneously. Once the qubit's state, it will return to a single state randomly, based on the squares of the probabilities. Where  $\alpha$  and  $\beta$  are probability amplitudes coefficients of the two-dimensional Hilbert space ( $\varphi$ ) and its relationship follows as in Eq. (3).

$$|\alpha|^2 + |\beta|^2 = 1 \quad (3)$$

The equations below present two-qubit states and their corresponding matrix columns. In the proposed architecture, we focused on the configuration of two qubits. The notations for the linear basis matrix are shown in Eqs. (4) and (5). As a response, they have been included in the proposed models.

$$0 \rightarrow |00\rangle = \begin{bmatrix} 1 \\ 0 \\ 0 \\ 1 \end{bmatrix}, \quad 1 \rightarrow |01\rangle = \begin{bmatrix} 1 \\ 0 \\ 0 \\ 0 \end{bmatrix}, \quad (4)$$

$$2 \rightarrow |10\rangle = \begin{bmatrix} 0 \\ 1 \\ 1 \\ 0 \end{bmatrix}, \quad 3 \rightarrow |11\rangle = \begin{bmatrix} 0 \\ 1 \\ 0 \\ 1 \end{bmatrix} \quad (5)$$

### 2.2.3. Quantum gates

Quantum gates, generally known as unitary operators, are the transformations that make up a quantum variant circuit. Every qubit quantum gate should satisfy the unitary operator's property, as shown in Eqs. (6) and (7). The single quantum bit gates Pauli-X, Pauli-Y, Pauli-Z, Hadmard, and rotational gates (from Eqs. (8) to (11)) can be used to operate the states in the quantum classifier [37]. Hadmard gates and rotational gates are applied in the proposed Pauli-Z model. They are represented in Eqs. (10) and (11). For the superposition of various states with equal computational basis state weights, the Hadmard gate is used. The Pauli-Z gate rotates by  $\pi$  radians around the z-axis and is controlled by phase shift.

$$\bigcup = e^{i\alpha} \left[ I \cos \theta/2 - i (\vec{\delta} \cdot \vec{n}) \sin \theta/2 \right] \quad (6)$$

$$\text{Here } \alpha = \pi/2, \theta = \pi \quad \bigcup = \delta \cdot \vec{n} \Rightarrow \delta_x n_x + \delta_y n_y + \delta_z n_z \quad (7)$$

The X gate can be described as a computational analog to the traditional NOT (or logical negation) operation. In computation, the states of the basis are altered. But the X-gate is not an actual quantum gate because it only changes the state logically in a computational sense.

$$\bigcup_{\text{pauli } X} = \delta_x = \begin{bmatrix} 0 & 1 \\ 1 & 0 \end{bmatrix}, \quad \text{where } \vec{n} = (1, 0, 0) \quad (8)$$

“-i” is a good mnemonic for placing the minus sign in the Y gate matrix. The Y-gate can be considered a combination of the X-gate and the Z-gate. From a computational point of view, we switch the 0 and 1 states and do a relative phase flip.

$$\bigcup_{\text{pauli } Y} = \delta_y = \begin{bmatrix} 0 & -i \\ i & 0 \end{bmatrix}, \quad \text{where } \vec{n} = (0, 1, 0) \quad (9)$$

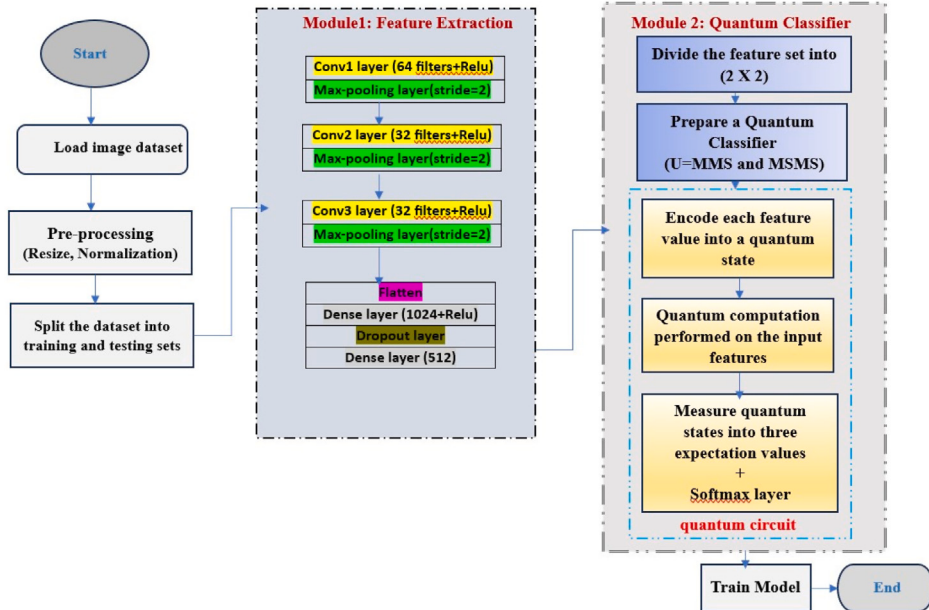


**Fig. 1.** The detailed workflows visual representation of Proposed Hybrid CCNN–Quantum Classifier Based Model.

The Z gate flips the phase of the  $|1\rangle$  state compared to the  $|0\rangle$  state from a computational point of view.

$$\bigcup_{\text{pauli}} Z = \delta_z = \begin{bmatrix} 1 & 0 \\ 0 & -1 \end{bmatrix}, \text{ where } n^\wedge = (0, 0, 1) \quad (10)$$

The Hadamard gate is one of the most interesting and practical of the standard gates. It causes a rotation of half a turn in the Bloch sphere.

$$\bigcup_{\text{Hadamard}} = \frac{1}{\sqrt{2}} \begin{bmatrix} 1 & 1 \\ 1 & -1 \end{bmatrix}, \text{ where } n^\wedge = \left( \frac{1}{\sqrt{2}}, 0, \frac{1}{\sqrt{2}} \right) \quad (11)$$

To rotate an object in Euclidean space, one uses rotation gates. According to Eq. (12), this single qubit rotates the points in the XY plane around an angle of  $\theta$  concerning the positive X-axis about the origin of two-dimensional data.

$$\text{Rotation}(\theta) = \begin{bmatrix} \cos \theta & -\sin \theta \\ \sin \theta & \cos \theta \end{bmatrix} \quad (12)$$

The proposed model applies a quantum Controlled-NOT (CNOT) gate to multi-qubit gates. Eq. (13) displays the linear matrix form. There are two inputs and two outputs on this two-qubit CNOT gate. As per Eqs. (14) and (15), the target (Second Qubit) is only flipped if the control qubit (First Qubit) is set to 1, and there is no effect on the change of the target qubit whenever the control qubit is set to 0. In other words, the inputs can be a linear superposition of  $|0\rangle$  and  $|1\rangle$ . The CNOT gate can change the quantum state. The matrix (in permutation matrix form) can be used to show the changes made by the CNOT gate.

$$\text{CNOT} = \begin{bmatrix} 1 & 0 & 0 & 0 \\ 0 & 1 & 0 & 0 \\ 0 & 0 & 1 & 0 \\ 0 & 0 & 0 & 1 \end{bmatrix} \Rightarrow I_4 \quad (13)$$

$$|10\rangle \underline{\text{CNOT}} |11\rangle \quad |11\rangle \underline{\text{CNOT}} |10\rangle \quad (14)$$

$$|00\rangle \underline{\text{CNOT}} |00\rangle \quad |01\rangle \underline{\text{CNOT}} |01\rangle \quad (15)$$

### 3. Proposed approach

This section explains the proposed model's structure, a new hybrid framework based on CCNN and Quantum Classifiers. The suggested framework constitutes two modules. The first module extracts the useful features over the chest X-ray images, and the second one classifies these features using quantum-based classifiers. The overall proposed hybrid CCNN–Quantum Classifier-based model's workflow is depicted in Fig. 1. Fig. 2 represents the generalized architecture of the proposed model for further classification, and Table 1 shows the complete summary of the ten experiments. Various classification algorithms like Support Vector Machine(SVM), K-Nearest Neighbor (KNN), Decision Tree(DT), Naive Bayes(NB), and AdaBoost.

#### 3.1. Module 1: Feature extraction

In this module, Custom CNN is used to extract the meaningful features from the chest X-ray images on the COVID-19\_Radiography\_Dataset [38] (Explained in Section 4). The suggested feature extraction approach comprises three convolution layers, three max-pooling layers, and two fully linked layers. In this architecture, the filters are 64, 64, and 32, with a kernel dimension of (2 2) and stride of 2. The convolutional layer employs kernels to conduct convolution operations on input features, extracting dependable and pivotal features from the scan images. The Rectified Linear Unit (ReLU) transformation function is the activation function in this architecture. The function mentioned above yields a value of 0 for any negative input while returning the same value as the input for any positive input. Max-pooling layer is employed to simplify computation by identifying and processing the most important and useful information. For each data sample, the X-ray image is passed to the feature extraction module, i.e., using the Custom CNN model. These features are flattened to send as input to classification modules. Here, we proposed two quantum circuit-based classifier models, MMS and MSMS. Now, the proposed classification models, such as MMS and MSMS, are trained on this flattened input by converting them into qubits. Finally, the classifiers classify the data into three classes COVID-19, Viral, and Normal.

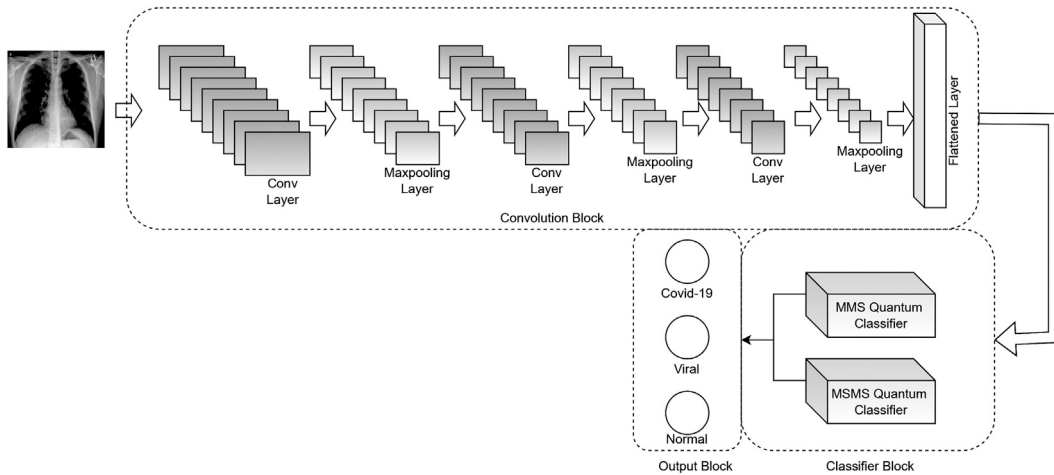


**Fig. 2.** Generalized Architecture of Proposed Hybrid CCNN–Quantum Classifier Based Model.

**Table 1**  
Summary of ten experiments with group models.

Experiment no.	Group models	
	Feature extraction model	Classification models
Expr 1	DenseNet121	SVM, KNN , DT, NB, AdaBoost
Expr 2	MobileNet	SVM , KNN , DT, NB,AdaBoost
Expr 3	Inception V3	SVM, KNN , DT, NB, AdaBoost
Expr 4	InceptionResNetV2	SVM, KNN , DT, NB, AdaBoost
Expr 5	ResNet50	SVM, KNN, DT, NB, AdaBoost
Expr 6	VGG16	SVM, KNN, DT, NB, AdaBoost
Expr 7	Xception	SVM, KNN, DT, NB, AdaBoost
Expr 8	ResNet18	MMS4,MMS4,MMS6,MSMS6(Qubit 4)
Expr 9	ResNet18	MMS4,MMS4,MMS6,MSMS6(Qubit 6)
Expr 10	CCNN	MMS4,MMS4,MMS6,MSMS6(Qubit 4)

### 3.2. Module 2: Quantum classifier

The goal of quantum classifiers is the same as that of classical classifiers. It involves entanglement, encoding qubits, and measuring the possibilities for final classification. The proposed quantum circuits act as classifiers because they contain concealed unitary operations that perform on encoded quantum states and produce the corresponding transformation values of entangled states. The measurement operation is performed to train the circuit. These measured probability values are adjusted as a training dataset to achieve the desired output. In subsequent subsections, the two proposed classifiers are discussed.

#### 3.2.1. Classification model 1: MMS (Multi-Multi-Single) quantum classifier

The input features obtained from module 1 are transmitted to the proposed processing unit (MMS). There are three layers in this model. The encoded layer (that converts classical features to quantum bits

or states), the variational circuit layer (which identifies the relationship between the qubits), and the measurement layer are all present (Converts the qubits back to classical).

**Encoded Layer:** In this layer, Hadmard gates are used to transform classical values to quantum states (Eq. (11)). These qubits then are encoded using a series of single rotational gates: RY, RX, RZ and RY for each block of the four-feature set. These are performed upon every qubit state with an angle around the X, Y, and Z axes. This gate sequence keeps the qubits in the standard superposition values  $|0\rangle$  and  $|1\rangle$ . The complexity of qubits and Quantum depth(Qdepth) in this approach are  $O(4)$  and  $O(6)$  respectively. The architecture of the encoded layer of MMS is shown in Fig. 3.

The single bit rotations RY, RX, and RZ are expressed as given in Eqs. (16) to (18).

$$RX(\phi) = \begin{bmatrix} \cos\left(\frac{\phi}{2}\right) & -i \sin\left(\frac{\phi}{2}\right) \\ -i \sin\left(\frac{\phi}{2}\right) & \cos\left(\frac{\phi}{2}\right) \end{bmatrix} \quad (16)$$

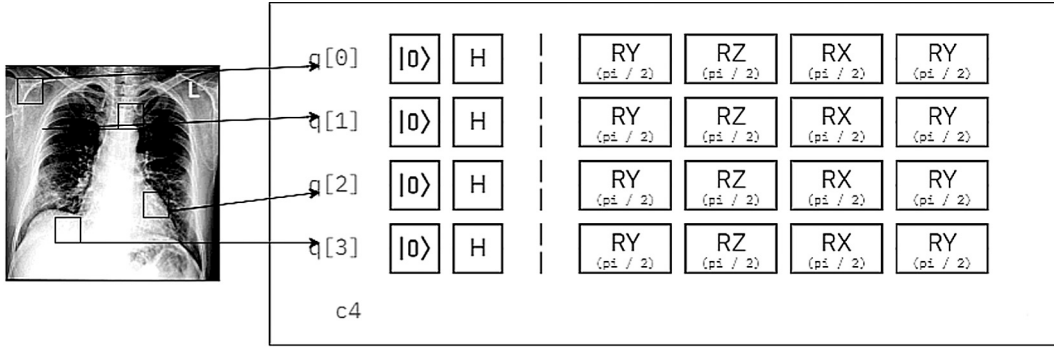


Fig. 3. Generalized architecture of Encoded layer in MMS Quantum Classifier.

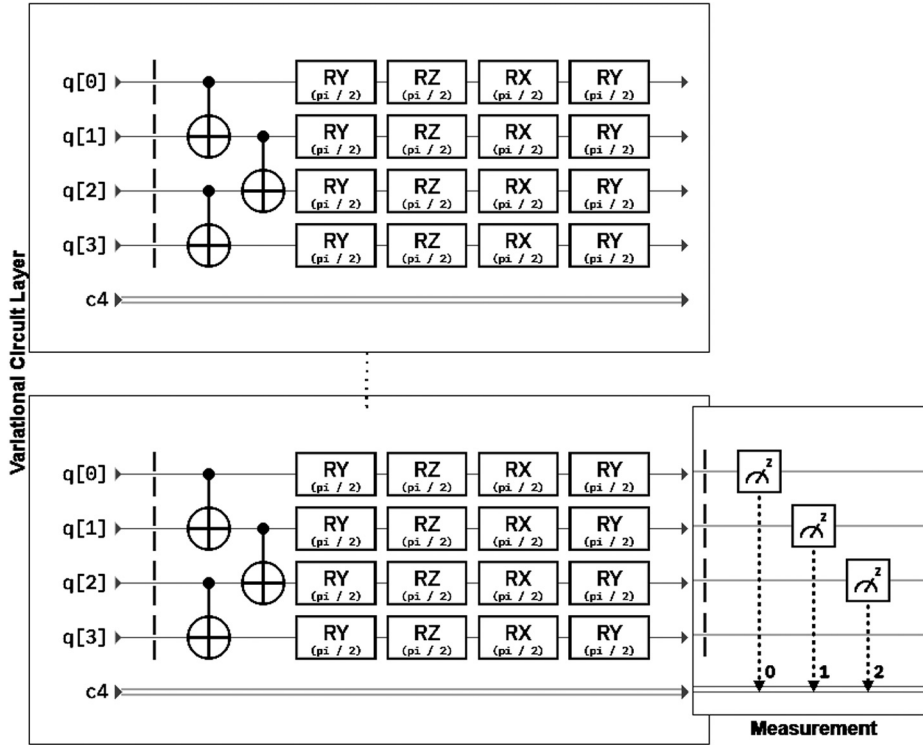


Fig. 4. Generalized variational circuit layer of MMS quantum classifier.

$$\text{RY}(\phi) = \begin{bmatrix} \cos\left(\frac{\phi}{2}\right) & -\sin\left(\frac{\phi}{2}\right) \\ \sin\left(\frac{\phi}{2}\right) & \cos\left(\frac{\phi}{2}\right) \end{bmatrix} \quad (17)$$

$$\text{RZ}(\phi) = \begin{bmatrix} \cos\left(\frac{\phi}{2}\right) & -\sin\left(\frac{\phi}{2}\right) \\ \sin\left(\frac{\phi}{2}\right) & \cos\left(\frac{\phi}{2}\right) \end{bmatrix} \quad (18)$$

**Variational Circuit Layer:** A multi-entangled CNOT gate and a single CNOT gate are used following the successful state encoding. The produced Qubits (Encoded Layer Output) are changed from one state to another by entanglement between even and odd quantum state indices. Here, three CNOT gates are used for entanglement: the first two are multi-CNOT gates, and the third is a single CNOT gate. The final is to apply and exhibit the entangled quantum states mapping with a set of four rotating gates (RY, RX, RZ and RY) presented in Fig. 4. Across the training phase, the variational circuit layer is repeated repeatedly. This repetition is done 4 and 6 times progressively in the proposed approach. This is referred to as Q-depth (Qdepth = 4 and Qdepth = 6).

---

**Algorithm 1: MULTI-MULTI-SINGLE QUBIT BASED MULTIPLE CLASS CLASSIFICATION**


---

**Input:**  $N$  - dimensional input features  $x^d \in \mathbb{R}^N$  that have been extracted and rescaled with  $\mathbb{R}^N$  between  $[0, 1]$

**Output:** Labelled Class for the feature vector  $y^d$  for the dataset  $D = (x^d, y^d)_{d=1}^D$

Setup:  $Data\_Quantumbits \leftarrow |0\rangle$ ;

$Q \leftarrow$  Depth of Quantum Variant Circuit ;

$\theta \leftarrow$  Classical computer optimization of quantum mechanics-based operating parameters;  $Data\_Quantumbits \leftarrow$  STATE CONFIGURATION

$(\text{RY}(x_i^d)\text{RZ}(x_i^d)\text{RX}(x_i^d)\text{RY}(x_i^d)) \forall i \in 1, 2, \dots, N$

for  $i \leftarrow 1$  to  $Q$  do

ENTANGLEMENT:  $\text{CNOT}[0, Data\_Quantumbits, 2]$  followed by another shifted  $\text{CNOT}[1, Data\_qubits, 2]$

$\text{RY}(\theta)\text{RZ}(\theta)\text{RX}(\theta)\text{RY}(\theta)$   $Data\_Quantumbits$  rotations

Values  $\leftarrow$  MEASUREMENT (PAULI-Z(DATA\_QUANTUMBITS))

Labelled Class  $\leftarrow$  SOFTMAX(Classical Values)

---

**Measurement Layer:** The measurement layer is commonly referred to as the decoding phase. Qubits were transformed into the required

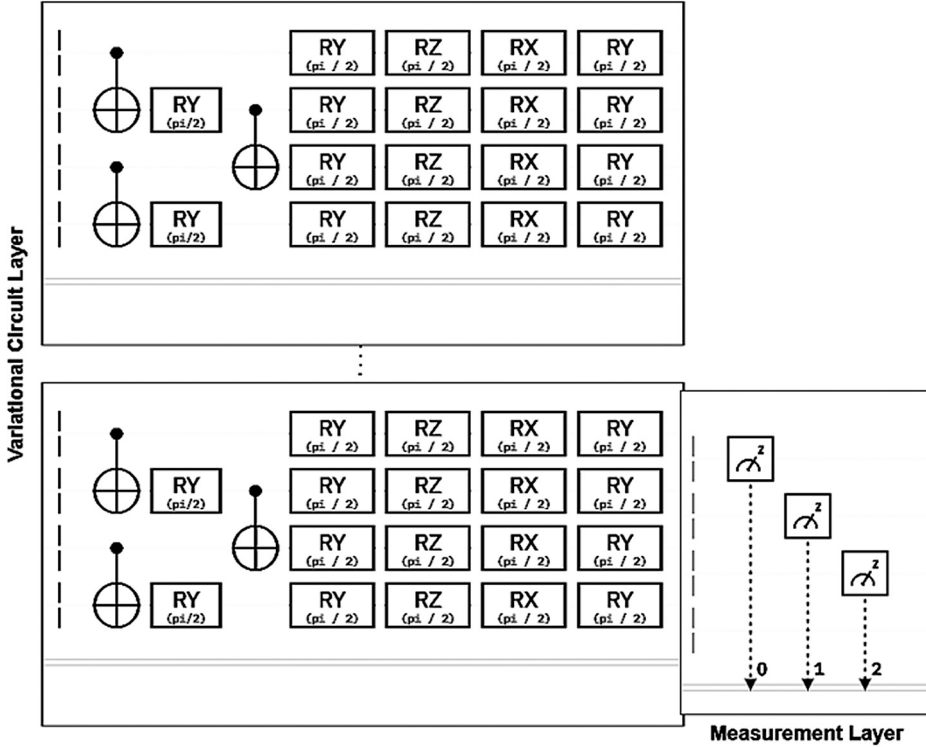


Fig. 5. Generalized variational circuit layer of MSMS quantum classifier.

output – classical values – by the Pauli-Z gate (Eq. (10)). This can be derived using the Dirac notation, where the class label is  $\langle E \rangle = |\psi\rangle E |\psi\rangle$ . The entire operation of the MMS classifier is shown in Algorithm 1 as a step-by-step process, called pseudocode.

### 3.2.2. Classification model 2: MSMS (Multi-Single-Multi-Single) quantum classifier

The three layers in this model are the Encoded Layer, Variational Circuit Layer, and Measurement Layer. The Encoded Layer and the Variable Circuit Layer are taken from Model 1 (MMS). Three CNOT gates are used for entanglement in this configuration of the variable circuit layer. The MSMS quantum classifier's entire architecture processes and makes decisions using quantum methods and quantum gates, followed by classical components, which are displayed in Fig. 5, and includes two Multi-Qubit CNOT gates, two Single-Qubit RY gates, and one CNOT gate. Throughout the training phase, the variational circuit layer is repeated multiple times. This repetition is performed by the proposed MSMS 4 and 6 times respectively, with Qdepth corresponding to 4 and 6. The complete multi-single classifier with the total number of layers is presented in Algorithm 2.

## 4. Experimental setup

### 4.1. Dataset collection and pre-processing

For this work, we used the COVID-19 Radiography Dataset9 (CRD) [38], which is a resource that is available publicly. The dataset is distributed in three class labels, namely COVID-19, Normal, and Viral are available in the form of X-ray images. This dataset consists of 15,153 X-ray images in total. This CRD validation is split into two parts, i.e., 20% for testing and 80% for training. Thus in training, we had 3,616 images for COVID-19, 10,192 images for normal, and 1,345 images for viral classes. For testing, we had 623 COVID images, 2,038

---

### Algorithm 2: MULTI-SINGLE-MULTI-SINGLE QUBIT BASED MULTIPLE CLASS CLASSIFICATION

---

**Input:**  $N$  - dimensional input data over the features vector  $x^d \in \mathbb{R}^N$  that have been extracted and rescaled with  $\mathbb{R}^N$  between  $[0, 1]$   
**Output:** Labelled Class for the feature vector  $y^d$  for the dataset  $D = (x^d, y^d)_{d=1}^D$   
**Setup:**  $Data\_Quantumbits \leftarrow |0\rangle$ ,  
 $Q \leftarrow$  Depth of Quantum Variant Circuit ;  
 $\theta \leftarrow$  Classical computer optimization of quantum mechanics-based operating parameters;  
 $Data\_Quantumbits \leftarrow$  STATE CONFIGURATION  
 $(RY(x_i^d)RZ(x_i^d)RX(x_i^d)RY(x_i^d)) \forall i \in 1, 2, \dots, N$   
**for**  $i \leftarrow 1$  **to**  $Q$  **do**  
  └ ENTANGLEMENT:  $CNOT[0, Data\_Quantumbits, 2]$   
  followed by  $RY(\theta)$ rotations then  $CNOT[1, Data\_Quantumbits, 2]$   
 $RY(\theta) RZ(\theta)RX(\theta)RY(\theta)$   $Data\_Quantumbits$  rotations  
  Values  $\leftarrow$  MEASUREMENT ( $Pauli-Z(Data\_qubits)$ )  
  Labelled Class  $\leftarrow$  SOFTMAX(Classical Values)

---

normal, and 269 viral X-ray images. To validate the trained images, they are transformed into a linear Min–Max approach using a scaling factor between  $[0, 1]$ . The complete description of the data distribution for this study is shown in Fig. 6. These characteristics help analysts and statisticians build the proposed model.

### 4.2. Configuration of the MMS quantum classifier architecture

Our encoding approach transforms the chosen classical features into four encoded qubits. The transformed and encoded qubits are then given to a constructed variable circuit. The MMS circuit is trained for this using two depths,  $Qdepth = 4$  and  $Qdepth = 6$ . Each layer of the proposed model is typically optimized using 19 parameters. That is when  $Qdepth$  is 1, containing three CNOT quantum gates and 16 single qubit rotations. The total number of parameters in the proposed classifier will be 72 when  $Qdepth = 4$  and 114 for  $Qdepth = 6$ , accordingly. Adam Optimizer is used to reduce the weights during

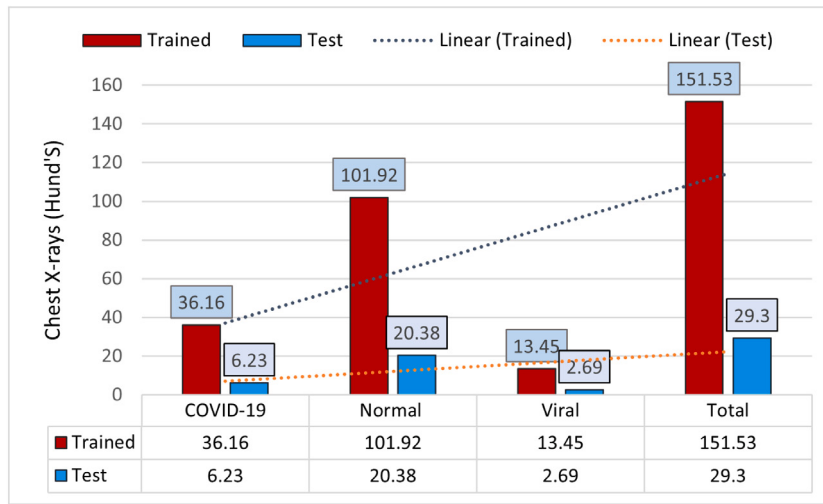


**Fig. 6.** Distribution of datasets in multiples of 100 for training and testing the proposed model.

**Table 2**  
Class C classification performance measurements.

Performance measurements	Range	Description
Accuracy	$\frac{TP+TN}{(TP+TN+FP+FN)}$	Number of Correctly class C classified
Specificity	$\frac{TN}{(TN+FP)}$	Number of Negative class C identified by classifier
Sensitivity	$\frac{TP}{(TP+FN)}$	Number of Positive class C identified by classifier
Precision	$\frac{TP}{(TP+FP)}$	Relation between Data labels with positive class C labels given by the classifier
FPR	$\frac{FP}{(TN+FP)}$	Relation between Data labels with negative class C labels given by the classifier
F1-Score	$\frac{2*TP}{(2*TP+FP+FN)}$	Relations between Data positive class C labels given by classifier

training using an initial learning rate of  $n = 0.004$  and is set to do so with the factor of gamma lr scheduler, which is designated as 0.1, every 10 epochs. Cross-entropy is built as a loss function to monitor the total cost value. The epoch number is defined as 30. The recommended model's performance measure is tabulated in [Table 4](#) while considering input qubits size 4 and 6. The accuracy between testing and training, and the cost throughout testing and training may be shown in this [Table 4](#). Moreover, both the trainable parameters and run-time are increased. The input qubit value is therefore set to 4 in the proposed models.

#### 4.3. Configuration of the MSMS quantum classifier architecture

The MSMS classifier's circuit Qdepth is set to 6. In this scenario, each layer uses 21 general input parameters. The total number of trainable parameters during the training phase is 126 whenever the Qdepth is 6, whereas it is 84 when it is 4. Cross-entropy is utilized to estimate the loss, and the Adam optimizer is used to update the weights during computation. The model is trained using a learning rate of  $n = 0.0004$  throughout 30 epochs. Since the performance doesn't change much as the amount of input qubits increases (as can be observed from [Table 4](#)), 4 qubits are used to train the model.

#### 5. Result analysis

To distinguish between COVID-19, normal, and viral images, the proposed model's performance is assessed using the nine experiments

listed in [Table 2](#). The quantum device simulator, accessible on the Pennylane Platform [39], is used for experimental simulations. Pytorch libraries have been used to implement all the performance reviews for Expr 1 to Expr 7 on Jupyter Notebook. The other three experiments, Expr 8, Expr 9 and Expr 10 were conducted on a new cross-platform called PennyLane. The most used metrics to validate the efficiency of classification problems and other significant results are accuracy, specificity, precision, sensitivity, FPR, F1-Score and AUC. These measures are defined using TP, TN, FP, and FN.

TP(True positive): The model correctly predicts class C and is labeled as C, Where C can be(COVID-19, Normal, or Viral).

TN(True Negative): The model correctly identifies C and is labeled as C,

FP(False Positive): The model incorrectly classifies C and labels it as C,

FN(False negative): The model incorrectly detects C and labels it as C.

The definition metrics are listed in [Table 2](#). The accuracy of multi-class classification is also compared using a confusion matrix.

#### 5.1. Experiment analysis:(Expr 1 - Expr 7)

The features extracted from various deep learning models are applied in Expr 1 through Expr 7 to train multiple machine learning classification models. The accuracy values from different classifiers and feature extraction approaches are tabulated in [Table 3](#) at their best epoch. The box-plot for the corresponding outputs with Precision, Sensitivity, and F1-Score is taken into consideration as shown in [Figs. 8a, 8b, 9c, 9d](#). These figures show the distribution of the above metrics across the various experimental conditions and models. The number

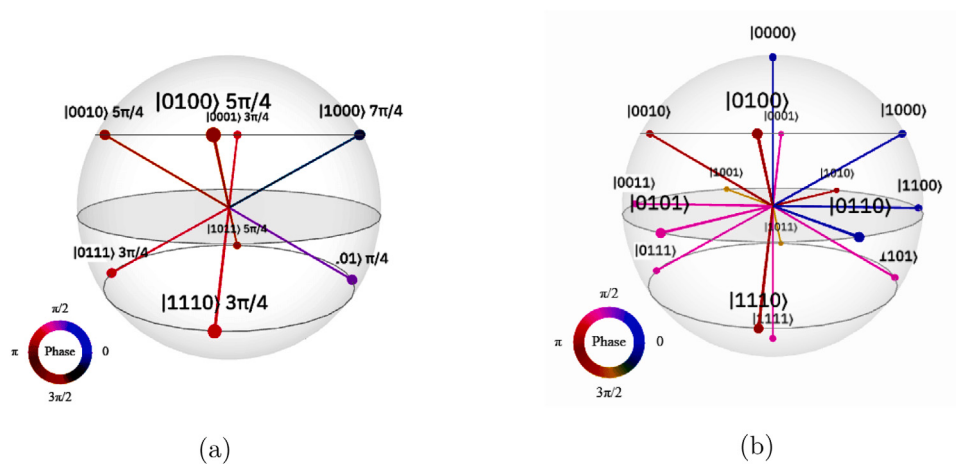


Fig. 7. Q-sphere (States and Phase angles) of proposed models: (a) MMS Classifier Model (b) MSMS classifier model.

Table 3

Comparison of accuracy between several feature extraction and classification models at the best epoch.

Feature extraction models	Classification models									
	AdaBoost (%)	Decision tree (%)	K-Nearest neighbors (%)	Naive Bayes (%)	Random forest (%)	Support vector machine (%)	MMS4 (Qubit 4/6) (%)	MSMS4 (Qubit 4/6) (%)	MMS6 (Qubit 4/6) (%)	MSMS6 Qubit4/6 (%)
Expr 1	58.4	84.6	93.1	82.4	95.4	96.2	64.2	65.2	66.0	67.1
Expr 2	67.2	82.5	94.4	88.7	93.5	97.5	88.7	89.2	89.8	88.2
Expr 3	74.2	86.4	87.1	85.2	88.5	90.1	86.4	88.4	87.2	89.1
Expr 4	71.2	82.5	87.2	83.8	90.5	92.8	84.2	86.4	88.1	84.2
Expr 5	76.2	81.5	92.6	78.2	82.5	73.6	94.1	95.2	95.1	92.4
Expr 6	64.3	83.4	95.5	84.2	94.2	97.1	92.1	93.4	94.1	93.5
Expr 7	55.2	81.2	89.4	83.5	91.2	94.6	87.7	89.4	88.9	86.5
Expr 8 & 9							97.7/94.1	98.3/96.7	99.0/97.2	97.1/94.1
Expr 10							97.9/95.2	98.9/98.1	99.4/98.2	98.1/97.9

of trainable parameters depends on model architecture, depth, and complexity. Fig. 10 shows the number of trainable parameters for each model, including the number of parameters and models. The model size is evaluated as the number of trainable parameters is computed on the type of computer. Where the 64-bit computer is considered for all the mathematical analysis.

- Expr 1 uses Densenet Model to extract the features and multiple machine learning models to classify them. Expr1 has the highest validation accuracy for the SVM classifier of 96.2% (from Table 3). From Figs. 8, 9, it provides precision of 94.2%, sensitivity of 91.0%, and F1-Score of 95.0%, correspondingly. AdaBoost classifier's lowest accuracy is measured at 58.4%. As per Fig. 10, this model has 7.9 million parameters in total, and the model size is 63MB.
- Expr 2 extracts the features by applying MobileNet and a classifier with distinct machine-learning models. It shows the SVM Classifier having the highest validation accuracy (97.5%) and the lowest validation accuracy (67.2%), respectively. According to Figs. 8a, 8b and 9c, 9d, it has a precision of 96.5%, a sensitivity of 92.0%, and an F1-Score of 91.1%. There are 1.7 million parameters in this model, and the size is 13MB.
- Expr 3 applies the Inception V3 model that extracts the features and other machine learning models to classify features. The SVM classifier in Expr 3 achieves the highest validation accuracy of 90.1% (taken from Table 3). According to Figs. 8 and 9, it has a precision of 89.2%, a sensitivity of 89.0%, and an F1-Score of 91.5%, respectively. AdaBoost's classifier achieves a minimum accuracy of 74.2%. According to Fig. 10, this model contains 6.4 million parameters in total and the model size is 51MB.

- The features are extracted by Expr4 using InceptionResNetV2 and a classifier with various machine learning models. The SVM Classifier achieves the highest validation accuracy at 92.8%. The precision, sensitivity, and F1-Score all reach 89.4%, 89.5%, and 94.5%, respectively. A minimum validation accuracy of 71.2% was obtained. This model has 5.2 million parameters and the size is 41MB.

- Expr 5 uses ResNet50 to extract the features and a classifier that uses a variety of machine learning models. The K-Nearest Neighbors Classifier has had the highest validation accuracy, which is 92.6%. It has a 95.5% F1-Score, 85.4% sensitivity, and 85.4% accuracy. The minimum validation accuracy was 73.6% for SVM Classifier, respectively. There are 25 million different parameters in this model and size is 200MB.

- Expr 6 extracts the features by using VGG16 and a classifier using different machine learning models. The SVM Classifier records the highest validation accuracy at 97.1%. The precision, sensitivity, and F1-Score are all at 94.1%, 92.2%, and 95.8%, respectively. The minimum validation accuracy for the AdaBoost Classifier is 64.3%. There are 13.8 million parameters in this model, and size of model is 110MB.

- In Expr 7, the features are extracted using Xception and a classifier that uses a variety of machine learning models. SVM Classifier has the highest validation accuracy, which is 94.6%. Their accuracy, sensitivity, and F1-Score are all 88.3%, respectively. The minimum validation accuracy for the AdaBoost Classifier is 55.2%. This model has 22 million trainable parameters, and size is 176MB.

Comparing the results of the above tests, Expr 1 to Expr 7, it is observed that Expr 2 is the best in terms of accuracy, specificity, precision, F1-Score, trainable parameters, and model size at the best epochs only.

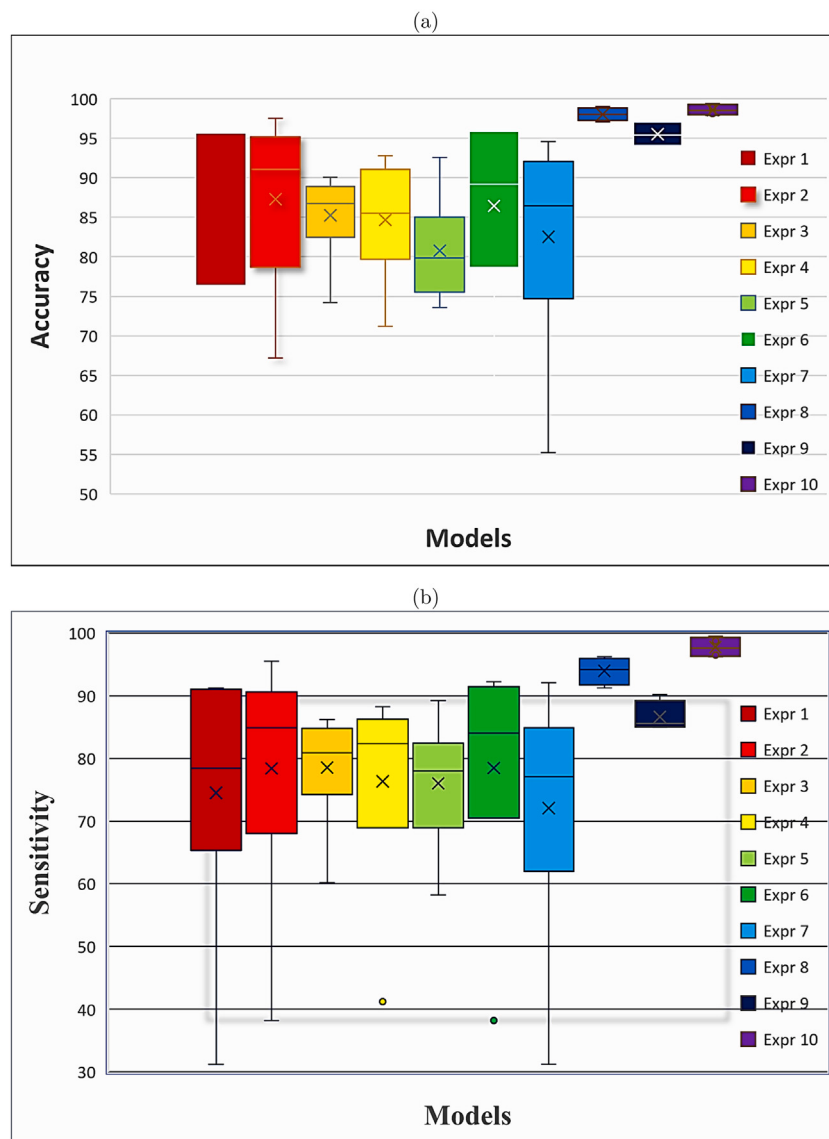


**Fig. 8.** Box plot comparison of ten respiratory lung diseases experimental models: (a) Accuracy (b) Sensitivity.

**Table 4**

A comparison of two proposed Quantum classifiers with varying numbers of input features is performed.

Classical network	Quantum network	Quantum depth	Qubit-4			Qubit-6			Training cost	Testing cost
			Training accuracy (Avg %)	Testing accuracy (Avg %)	Training cost	Testing cost	Training accuracy (Avg %)	Testing accuracy (Avg %)		
ResNet 18	MMS	4	90.4	92.1	0.3	0.2	90.1	92.2	0.3	0.2
ResNet 18	MSMS	4	90.5	91.4	0.3	0.2	90.6	91.3	0.1	0.1
ResNet 18	MMS	6	91.1	92.6	0.2	0.2	91.4	92.1	0.1	0.1
ResNet 18	MSMS	6	90.1	97.1	0.3	0.2	90.4	97.4	0.2	0.2
CCNN	MMS	4	92.4	93.8	0.2	0.3	92.1	93.1	0.1	0.2
CCNN	MSMS	4	94.2	97.2	0.07	0.09	94.4	97.4	0.07	0.08
CCNN	MMS	6	96.3	98.1	0.07	0.08	95.4	98.5	0.08	0.17
CCNN	MSMS	6	92.3	93.7	0.2	0.3	92.4	94.4	0.2	0.2

### 5.2. Experiment analysis: (Expr 8)

- In this experiment, using features taken from ResNet-18, we compared the performance of MMS and MSMS with Qdepths of 4 and 6 for qubit 4 (shown in Table 5). It has already been proven through analysis of Table 4 data that Qubit 6 performs similarly to Qubit-4. As a result, Qubit 4 is the only point in which the metrics accuracy, sensitivity, precision, F1-Score, FPR, AUC are

measured. At first, the Hybrid MMS4 analysis shows an accuracy of 86%, a sensitivity of 86%, a specificity of 97.5%, a precision of 90.8%, an F1-Score of 88.3%, FPR of 0.09% and AUC is 0.85. The higher values were also achieved by the Normal and Viral classes. The average of this model's training and testing accuracy was 90.4% and 92.1%, respectively, as shown in Table 6. The results also indicate that the costs involved with training and testing were relatively low, at 0.30 and 0.20, respectively.

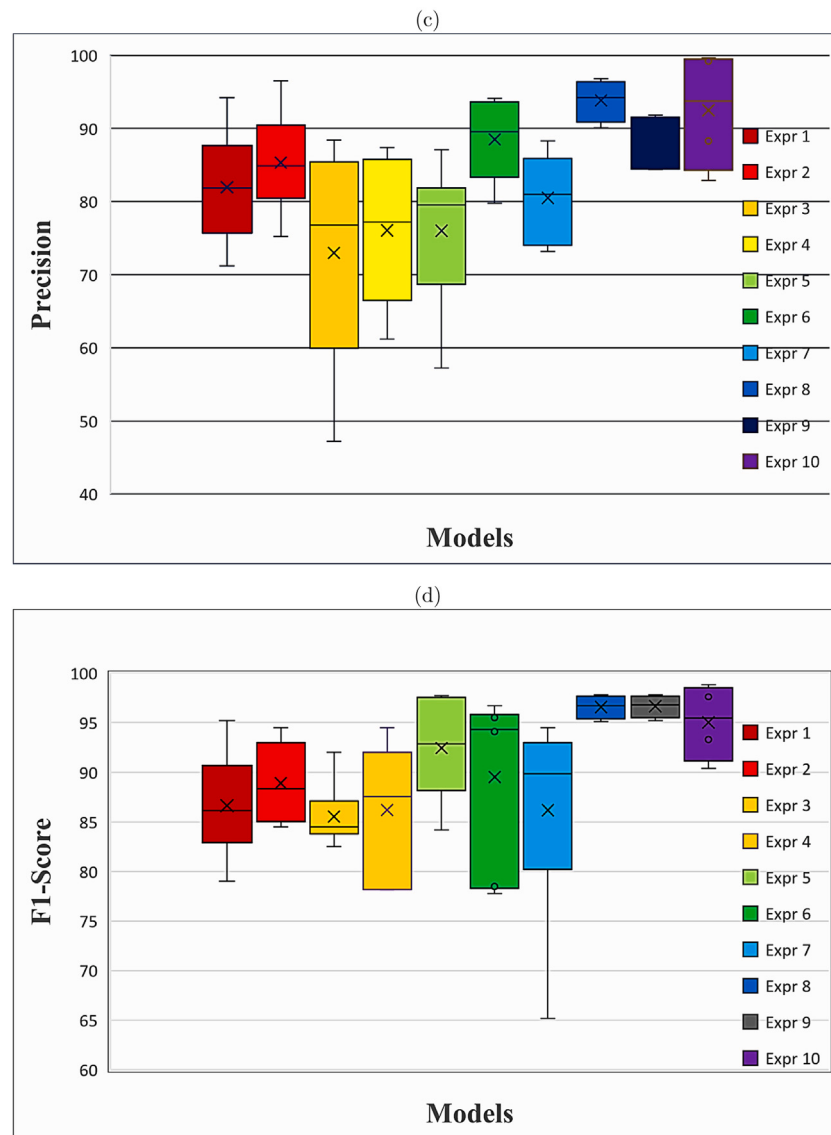


Fig. 9. Box plot comparison of ten respiratory disease experimental models: (c) Precision (d) F1-Score.

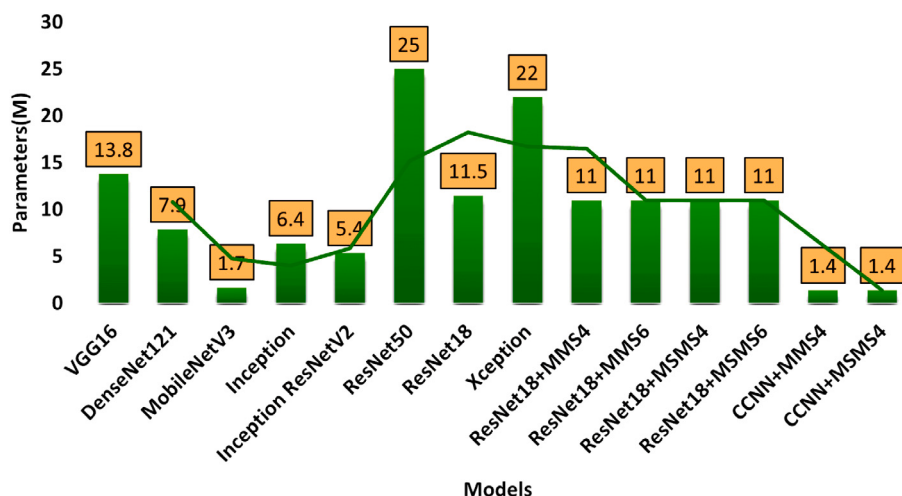


Fig. 10. Comparison of trainable parameters between literature and proposed models.

**Table 5**

Comparison results of respiratory diseases Classification Using a Hybrid CCNN and Quantum Classifier(Qubit-4)with existing Models.

Hybrid C-Q models/existed models	Image type/size	Accuracy (%)	Sensitivity (%)	Specificity (%)	Precision (%)	F1-Score (%)	FPR (%)	AUC
Ref [40]	<i>COVID-19-3,616</i>	95.2	97.2	—	98.1	98.3	—	—
	<i>Normal-10,192</i>	95.2	98.2	—	89.0	93.0	—	—
	<i>Viral-1345</i>	95.2	97.1	—	97.8	92.0	—	—
Ref [41]	<i>COVID-19-3,616</i>	97.4	95.9	97.0	95.9	95.8	—	—
	<i>Normal-10,192</i>	—	—	—	—	—	—	—
	<i>Viral-1345</i>	—	—	—	—	—	—	—
Ref [42]	<i>COVID-19-3,616</i>	96.3	94.3	96.5	92.6	93.5	—	—
	<i>Normal-10,192</i>	—	—	—	—	—	—	—
	<i>Viral-1345</i>	—	—	—	—	—	—	—
Ref [43]	<i>COVID-19-3,616</i>	96.3	96.5	—	97.0	96.8	1.00	—
	<i>Normal-10,192</i>	—	—	—	—	—	—	—
	<i>Viral-1345</i>	—	—	—	—	—	1.00	—
Ref [29]	<i>COVID-19-3,616</i>	96.1	96.5	—	97.2	97.5	—	—
	<i>Normal-10,192</i>	—	—	—	—	—	—	—
	<i>Viral-1345</i>	—	—	—	—	—	1.00	—
ResNet18 + MMS4	<i>COVID-19-3,616</i>	<b>86.0</b>	<b>86.0</b>	97.5	90.8	88.3	0.09	0.85
	<i>Normal-10,192</i>	<b>97.2</b>	97.2	87.6	94.7	91.0	<b>0.12</b>	0.89
	<i>Viral-1345</i>	88.8	88.8	99.8	97.5	98.6	0.01	0.65
ResNet 18 + MMS6	<i>COVID-19-3,616</i>	85.0	85.0	<b>97.9</b>	<b>91.8</b>	<b>88.4</b>	<b>0.02</b>	0.97
	<i>Normal-10,192</i>	97.1	<b>97.5</b>	86.8	94.4	90.4	0.13	0.84
	<i>Viral-1,345</i>	88.2	90.7	<b>99.8</b>	<b>98.7</b>	<b>99.2</b>	<b>0.01</b>	0.68
ResNet18 + MSMS4	<i>COVID-19-3,616</i>	85.0	84.7	97.1	89.0	86.8	0.02	0.91
	<i>Normal-10,192</i>	96.7	96.7	<b>88.0</b>	<b>94.8</b>	<b>91.2</b>	0.13	0.84
	<i>Viral-1,345</i>	92.5	92.5	99.6	96.5	98.0	0.03	0.53
ResNet18 + MSMS6	<i>COVID-19-3616</i>	84.0	84.4	97.6	90.6	87.4	0.02	0.91
	<i>Normal-10,192</i>	97.1	97.0	87.8	94.8	91.1	0.12	0.85
	<i>Viral-1,345</i>	<b>94.7</b>	<b>94.7</b>	99.6	96.5	98.0	0.03	0.52
CCNN + MMS6	<i>COVID-19-3616</i>	98.4	96.2	99.5	98.3	97.3	0.004	0.97
	<i>Normal-10,192</i>	98.4	98.5	98.1	99.2	98.8	0.018	0.98
	<i>Viral-1,345</i>	<b>98.8</b>	<b>98.7</b>	98.8	88.4	93.3	0.015	0.98
CCNN + MSMS4	<i>COVID-19-3616</i>	98.9	96.5	99.6	98.7	97.6	0.003	0.91
	<i>Normal-10,192</i>	97.1	97.0	87.8	94.8	91.1	0.12	0.92
	<i>Viral-1,345</i>	<b>98.4</b>	<b>99.5</b>	98.3	82.9	90.4	0.017	0.98

**Table 6**

Comparison of different existing models with Hybrid CCNN–Quantum Classifier based Models.

Feature extraction + classifier	Quantum depth	Trainable parameters (Total)	Model size (MB/KB)	Training accuracy (avg%)	Testing accuracy (avg%)	Training cost	Test cost
Ref [41]	NA	—	—	95.9	98.2	0.2	0.1
Ref [42]	NA	—	—	96.3	98.1	0.2	0.1
Ref [43]	NA	—	—	95.7	95.3	0.2	0.2
Ref [29]	NA	—	—	96.1	98.3	0.3	0.2
Ref [44]	NA	—	—	82.2	87.1	0.3	0.5
VGG-16	NA	13.8M	110MB	84.8	90.1	0.2	0.2
Inception Net	NA	6.4M	51MB	81.9	89.9	0.2	0.2
MobileNet V3	NA	1.7M	14MB	87.9	88.14	0.3	0.2
ResNet50	NA	25M	200MB	89.2	90.4	0.3	0.2
ResNet-18	NA	11.5M	92MB	89.9	91.9	0.2	0.2
ResNet-18 + MMS	4	11M	88MB	90.4	92.1	0.3	0.2
	6	11M	88MB	<b>91.1</b>	<b>92.6</b>	<b>0.2</b>	<b>0.2</b>
ResNet-18 + MSMS	4	11M	88MB	<b>90.5</b>	<b>91.4</b>	<b>0.3</b>	<b>0.2</b>
	6	11M	88MB	90.1	90.8	0.3	0.2
CCNN + MMS	4	1.4M	11MB	92.4	93.8	0.2	0.3
	6	1.4M	11MB	<b>96.3</b>	<b>98.1</b>	<b>0.07</b>	<b>0.09</b>
CCNN + MSMS	4	1.4M	11MB	94.2	<b>97.2</b>	<b>0.07</b>	<b>0.08</b>
	6	1.4M	11MB	92.3	93.7	0.2	0.2

- The second model, MMS6 predicts the disease, in terms of accuracy, sensitivity, specificity, precision, F1-score, and AUC with 85.0%, 85.0%, 97.9%, 91.8%, 88.4%, 0.02%, and 0.97, respectively. During the training and testing stages, this hybrid model had average accuracy levels of 91.1% and 92.6%. Both training and testing have a cost of 0.02 and 0.02, respectively. The Normal and Viral classes also achieved the higher values.
- The proposed MSMS4 achieved accuracy of 85.0%, sensitivity of 84.7%, specificity of 97.1%, precision of 89.0%, F1-Score of 86.8%, FPR of 0.02% and AUC value of 0.91. The models also

attained average accuracy of 90.5% and 91.4%, respectively, during the training and testing processes. Training evaluation costs are 0.3% and testing evaluation cost is 0.2%. The better values were also achieved by the Normal and Viral classes.

- Final results for the MSMS6 model include 84.0% accuracy, 84.4% sensitivity, 97.6% specificity, 90.6% precision, 87.4% F1-Score, 0.03% FPR and AUC is 0.91 for the COVID-19 class. The outputs of the average both training and testing accuracy are 90.1% and 90.8% for multiple classes (COVID-19, Normal, and Viral), respectively. The computational costs of training and

Figure 11 consists of six confusion matrices labeled (a) through (f). Each matrix has 'Actual' on the left and 'Predicted' at the top. The columns represent 'Covid-19', 'Normal', and 'Viral'. The rows represent 'Covid-19', 'Normal', and 'Viral'. The values in the cells indicate the count of correctly predicted samples (white), misclassified samples (gray), and false positives (dark gray).

		Predicted					Predicted				
		Covid-19	Normal	Viral			Covid-19	Normal	Viral		
Actual	Covid-19	538	84	1	Actual	526	95	2			
	Normal	53	1981	4		Normal	53	1978			7
	Viral	4	26	239		Viral	1	13			255

(a)

		Predicted					Predicted				
		Covid-19	Normal	Viral			Covid-19	Normal	Viral		
Actual	Covid-19	530	93	0	Actual	613	8	2			
	Normal	46	1989	3		Normal	15	2022			1
	Viral	1	24	244		Viral	9	22			238

(d)

		Predicted					Predicted				
		Covid-19	Normal	Viral			Covid-19	Normal	Viral		
Actual	Covid-19	528	90	5	Actual	615	8	0			
	Normal	62	1972	4		Normal	12	2024			1
	Viral	3	17	249		Viral	10	36			223

(b)

		Predicted					Predicted				
		Covid-19	Normal	Viral			Covid-19	Normal	Viral		
Actual	Covid-19	530	93	0	Actual	613	8	2			
	Normal	46	1989	3		Normal	15	2022			1
	Viral	1	24	244		Viral	9	22			238

(c)

		Predicted					Predicted				
		Covid-19	Normal	Viral			Covid-19	Normal	Viral		
Actual	Covid-19	528	90	5	Actual	615	8	0			
	Normal	62	1972	4		Normal	12	2024			1
	Viral	3	17	249		Viral	10	36			223

(e)

		Predicted					Predicted				
		Covid-19	Normal	Viral			Covid-19	Normal	Viral		
Actual	Covid-19	530	93	0	Actual	613	8	2			
	Normal	46	1989	3		Normal	15	2022			1
	Viral	1	24	244		Viral	9	22			238

(f)

**Fig. 11.** Details of the confusion matrix of proposed models based on Qubit-4: (a) ResNet18 with MMS4 Model (b) ResNet18 with MMS6 Model (c) ResNet18 with MSMS4 Model (d) ResNet18 with MSMS6 Model (e) CNN with MMS6 Model (f) CNN with MSMS4 Model.

testing were reported as 0.3% and 0.2%, respectively. The best values were also achieved by the Normal and Viral classes.

- Additionally, Table 6 provided a comprehensive comparison between the proposed four hybrid quantum classifier models and some existing models such as VGG-16, Inception Net, MobileNet V3, ResNet50, and ResNet18. The number of trainable parameters and model size is very less compared with other existing models.
- Both training and testing comparative curves of the proposed hybrid models with epochs (30) are shown in Figs. 12 and 13. The confusion matrix for each of the six individual models is shown in Fig. 11a, 11b, 11c, 11d, 11e, 11f.
- Reviewing the Tables 4, 5, and 6, as well as the Figs. 8, 9, and 11 shown the different metrics for detecting the Normal, Viral, and COVID are found to be best by MMS6 and MSMS4.
- We also validated the model on the real-time quantum processor IBMQ-QASM to conduct the proposed circuit quantum MMS classifier. The highest and lowest measurement results of qubit state  $|0100\rangle, |0111\rangle$  are 140 and 115, respectively, according to the Q-sphere shown in Fig. 7a. The overall timeline is 965ms. Moreover, the IBMQ-QASM real-time quantum processor verifies and approves the MSMS classifier circuit. The states and phase

angles of the qubit state with maximum and minimum frequencies are shown in Fig. 7b as  $|0010\rangle, |0001\rangle$  are 170 and 115, respectively.

### 5.3. Experiment analysis: Expr 9

Four hybrid models are being considered in this experiment depending on qubit 6 for respiratory disease detection. In Case 1, the MMS4 model attained a validation accuracy of 92.2% and an average computational cost of 0.2%. During the training and testing stages, MSMS 4 achieves an accuracy of 91.3% at a computational cost of 0.1%. However, MMS6 was able to reduce the cost to 0.1% while also achieving an accuracy rate of 92.1%. Finally, MSMS6 provided validation accuracy rates of 97.4%, 0.2%, and average cost, respectively. The outcomes comparing various proposed models with various input feature values were displayed in Table 4.

The result of these models for each experiment is shown in Table 3. In this regard one of the best accuracy is 97.2%, the precision of 97.5%, the sensitivity of 99.8%, the computational cost of 0.1%, F1-score of 99.2% and AUC value of 0.91 are recorded for both MMS6 and MSMS4. These models perform better than compared to the other existing models for various respiratory diseases. The number of trainable parameters

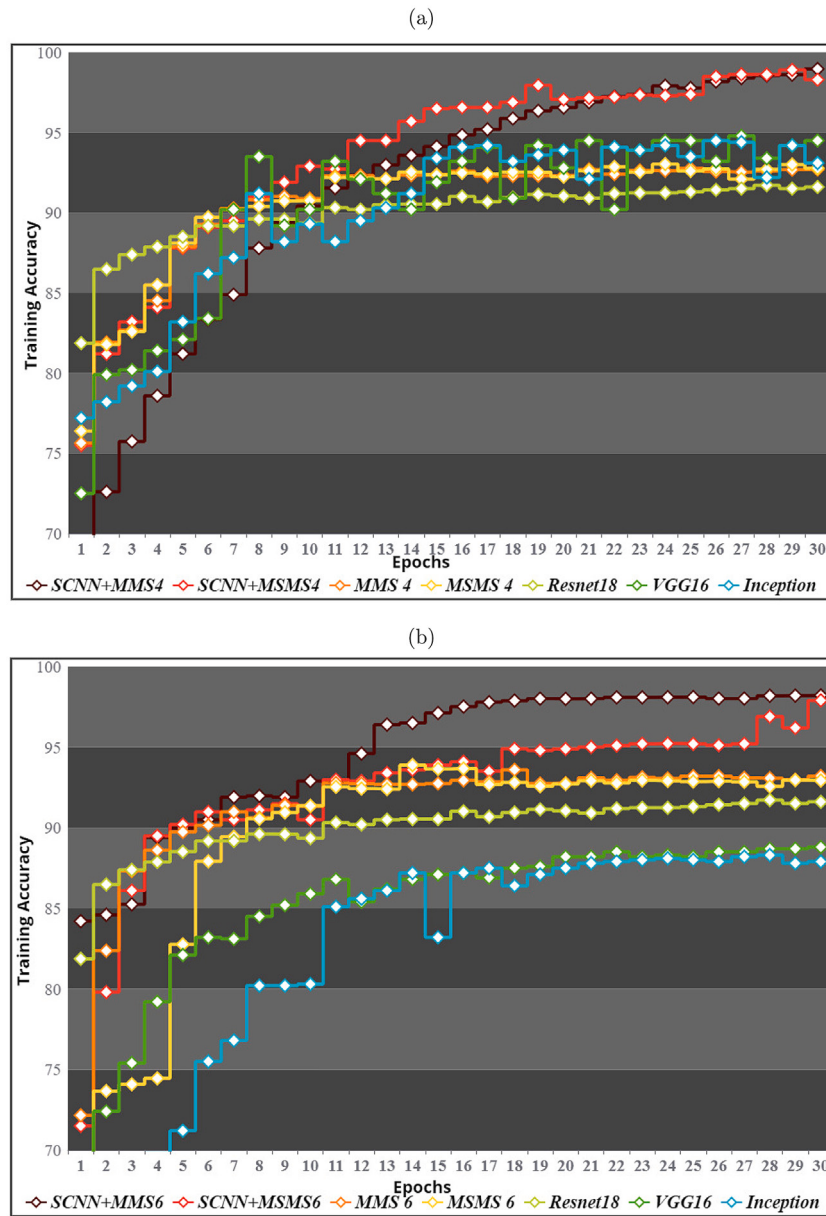


**Fig. 12.** The proposed models training and testing accuracy comparisons using Qubit-4:(a)Training accuracy of CCNN with MMS4 and MSMS4 Model (b)Training accuracy of CCNN with MMS6 and MSMS6 Model.

of these models is 11M, and the model size is 88MB. The box plot of various measure performances between experiment 9 with other experiments is shown in Figs. 8 and 9.

#### 5.4. Experiment analysis: Expr 10

- In this experiment, using features taken from CCNN, we compared the performance of MMS and MSMS with Qdepth of 4 and 6 for qubit 4 (shown in Table 5). It has already been proven through analysis of Table 4 data that Qubit 6 performs similarly to Qubit-4. As a result, Qubit 4 is the only point in which the metrics accuracy, sensitivity, precision, F1-Score, FPR, and AUC are measured. At first, the Hybrid CCNN with MMS6 analysis shows COVID-19 with an accuracy of 98.4%, a sensitivity of 96.2%, a specificity of 99.5%, a precision of 98.3%, an F1-Score of 97.3%, an FPR as 0.004% and AUC is 0.97. The model also shows the normal with an accuracy of 98.4%, a sensitivity of 98.5%, specificity of 98.1%, a precision of 99.2%, an F1-Score of 98.8%,

an FPR as 0.018% and AUC is 0.98. The Normal and Viral classes also achieved higher values.

- The proposed MSMS4 achieved an accuracy of 98.9%, a sensitivity of 96.5%, a specificity of 99.6%, precision of 98.7%, an F1-Score of 97.6%, an FPR of 0.003% and AUC value is 0.91. The models also attained average accuracies of 94.2% and 97.2% respectively, during the training and testing processes. Training evaluation costs are 0.07% and testing evaluation cost is 0.08%. The higher AUC values of 0.92 and 0.98 are obtained for Normal and Viral classes respectively.
- Additionally, Table 6 provided a comprehensive comparison between the proposed four hybrid quantum classifier models with other hybrid classical-quantum models and also some existing models such as VGG-16, Inception Net, MobileNet V3, ResNet50, and ResNet18. The proposed model shows significant results in terms of cost, number of trainable parameters (1.4M), and model size (11MB). Hence the computation power is reduced.

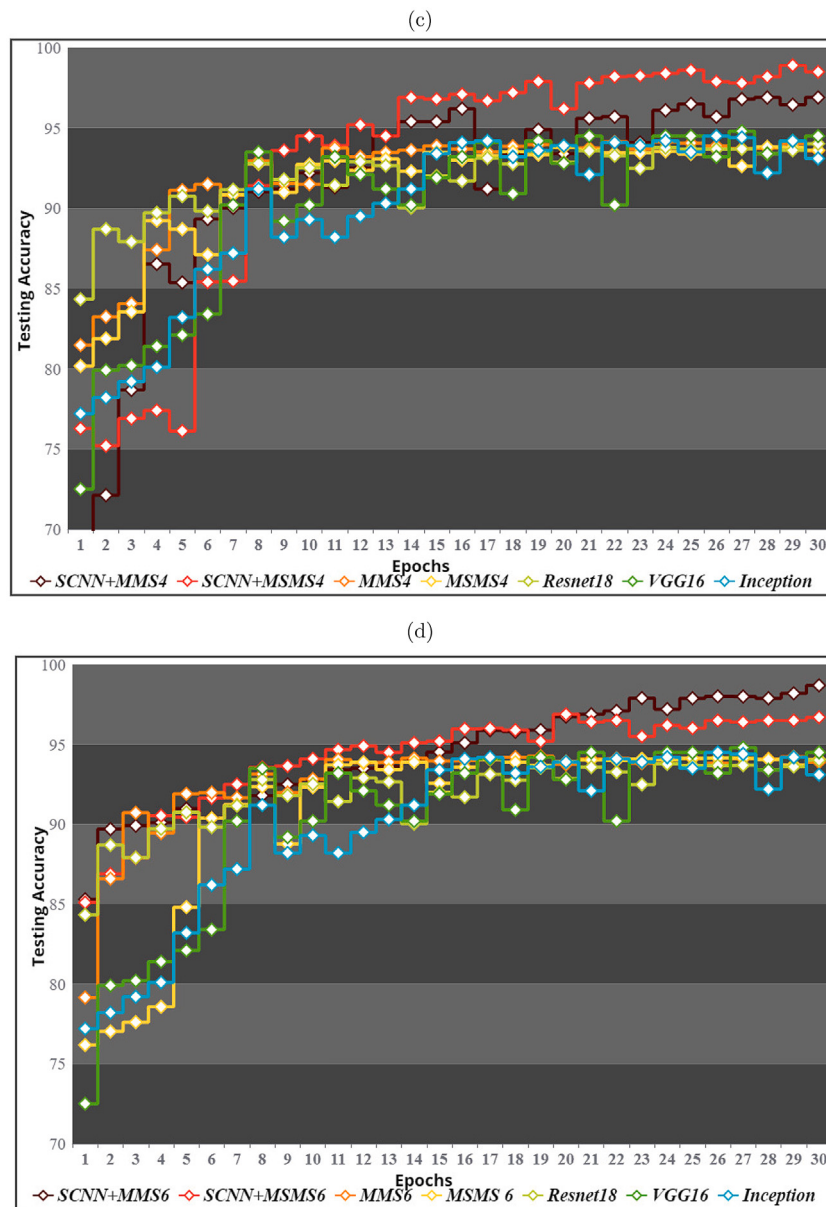


**Fig. 13.** The proposed models training and testing accuracy comparisons using Qubit-4: (c) Testing accuracy of CCNN with MMS4 and MSMS4 Model (d) Testing accuracy of CCNN with MMS6 and MSMS6 Model.

- Figs. 11a, 11b, 11c, 11d, 11e, and 11f display the confusion matrix for each of the six models based on their predictions and class labels at qubit-4 for different respiratory diseases. The comparison plot of the training and test accuracies between both the standard models and each proposed hybrid model at 30 epochs is shown in Figs. 12a, 12b and 13c, 13d.
- Reviewing the Table 4, 5, and 6, as well as the Figs. 8a, 8b, 9c, 9d, 11a, 11b, 11c, 11d, 11e, 11f, 12a, 12a and 13c, 13d shown the various metrics for detecting the Normal, Viral, and COVID are found to be best by CCNN with MMS6 and MSMS4.

Results of proposed models for each experiment are shown in Table 3. In terms of overall accuracy, precision, sensitivity, computational cost, F1-Score, AUC, number of trainable parameters and model size, CCNN with MMS6 and CCNN with MSMS4 perform better than compared to the above existing models for the respiratory disease classes. The box plot from several measuring performances between the expr 10 and other experiments is shown in Figs. 8a, 8b and 9c, 9d.

## 6. Conclusion and future directions

In this article, we proposed a respiratory lung disease detection system based on the Hybrid CCNN and Quantum classifier-based transfer learning model, which combines the CCNN network with quantum classifiers for extraction of features and multi disease classification, respectively. Upon experiments, it is confirmed that the proposed MMS and MSMS quantum classifiers can accomplish the classification task for respiratory disorders more effectively with optimal trainable parameters. This article conducted various experiments on the real time IBMQ-QASM quantum processor and standard default qubit simulators with Qubits of 4 and 6, respectively. The results of the proposed CCNN with MMS6 and MSMS4 classifiers showed more promising outcomes and were more optimized than other standard deep learning models. In contrast to existing encoding techniques, our developed encoding approach used in quantum classifiers has a much smaller size, lower computing costs, and requires fewer trainable parameters. This work

also introduces an alternative idea regarding integrating classical machine learning with quantum processors. The scope of this article can be expanded to extend the number of qubits and design various encoding schemes for data augmentation, handling more challenging medical datasets, and multi-class disease detection systems.

### CRediT authorship contribution statement

**G.V. Eswara Rao:** Conceptualization, Methodology, Investigation, Writing – original draft, Supervision. **Rajitha B.:** Conceptualization, Methodology, Software, Infrastructure, Investigation, Writing – original draft. **Parvathaneni Naga Srinivasu:** Conceptualization, Methodology, Software, Investigation, Validation, Visualization, Writing – original draft. **Muhammad Fazal Ijaz:** Conceptualization, Software, Methodology, Investigation, Validation, Visualization, Writing – original draft. **Marcin Woźniak:** Conceptualization, Software, Validation, Investigation, Writing – original draft.

### Declaration of competing interest

The authors declare that they have no known competing financial interests or personal relationships that could have appeared to influence the work reported in this paper.

### Data availability

Data will be made available on request.

### References

- [1] C.L. Atzrodt, I. Maknojia, R.D. McCarthy, T.M. Oldfield, J. Po, K.T. Ta, H.E. Stepp, T.P. Clements, A guide to COVID-19: a global pandemic caused by the novel coronavirus SARS-CoV-2, *FEBS J.* 287 (17) (2020) 3633–3650.
- [2] L. Ni, F. Ye, M.L. Cheng, Y. Feng, Y.Q. Deng, H. Zhao, P. Wei, J. Ge, M. Gou, X. Li, L. Sun, Detection of SARS-CoV-2-specific humoral and cellular immunity in COVID-19 convalescent individuals, *Immunity* 52 (6) (2020) 971–977.
- [3] Y.B. De Bruin, A.S. Lequarre, J. McCourt, P. Clevestig, F. Pigazzani, M.Z. Jeddi, C. Colosio, M. Goulart, Initial impacts of global risk mitigation measures taken during the combatting of the COVID-19 pandemic, *Saf. Sci.* 128 (2020) 104773.
- [4] K. Dham, S.K. Patel, K. Sharun, M. Pathak, R. Tiwari, M.I. Yatoo, Y.S. Malik, R. Sah, A.A. Rabaan, P.K. Panwar, K.P. Singh, SARS-CoV-2 jumping the species barrier: Zoonotic lessons from SARS, MERS and recent advances to combat this pandemic virus, *Travel Med. Infect. Dis.* 37 (2020) 101830.
- [5] A. Rivas, Drones and artificial intelligence to enforce social isolation during covid-19 outbreak, *Medium Towards Data Sci.* 26 (2020).
- [6] C. Zheng, X. Deng, Q. Fu, Q. Zhou, J. Feng, Deep learning-based detection for covid-19 from chest ct using weak label, 2020, medRxiv.
- [7] T. Mihara, Y. Nishimura, Y. Shimizu, H. Nishiyama, G. Yoshikawa, H. Uehara, P. Hingamp, S. Goto, H. Ogata, Linking virus genomes with host taxonomy, *Viruses* 8 (3) (2016) 66.
- [8] Alfredo Canziani, Adam Paszke, Eugenio Culurciello, An analysis of deep neural network models for practical applications, 2016, arXiv preprint [arXiv:1605.07678](https://arxiv.org/abs/1605.07678).
- [9] K. Ch'ng, J. Carrasquilla, R.G. Melko, E. Khatami, Machine learning phases of strongly correlated fermions, *Phys. Rev. X* 7 (031038) (2017) 10–1103.
- [10] J. Biamonte, P. Wittek, N. Pancotti, P. Rebentrost, N. Wiebe, S. Lloyd, Quantum machine learning, *Nature* 549 (7671) (2017) 195–202.
- [11] C. Ciliberto, M. Herbster, A.D. Ialongo, M. Pontil, A. Rocchetto, S. Severini, L. Wossnig, Quantum machine learning: a classical perspective, *Proc. R. Soc. A* 474 (2209) (2018) 20170551.
- [12] G. Verdon, M. Broughton, J.R. McClean, K.J. Sung, R. Babbush, Z. Jiang, et al., Learning to learn with quantum neural networks via classical neural networks, 2019, arXiv preprint [arXiv:1907.05415](https://arxiv.org/abs/1907.05415).
- [13] Edward Farhi, Hartmut Neven, Classification with quantum neural networks on near term processors, 2018, arXiv preprint [arXiv:1802.06002](https://arxiv.org/abs/1802.06002).
- [14] M. Schuld, N.N. Killoran, Quantum machine learning in feature Hilbert spaces, *Phys. Rev. Lett.* 122 (4) (2019) 040504.
- [15] R. McClean Jarrod, et al., The theory of variational hybrid quantum-classical algorithms, *New J. Phys.* 18 (2) (2016) 023023.
- [16] Nathan Killoran, et al., Continuous-variable quantum neural networks, *Phys. Rev. Res.* 1 (3) (2019) 033063.
- [17] Alejandro Perdomo-Ortiz, et al., Opportunities and challenges for quantum-assisted machine learning in near-term quantum computers, *Quantum Sci. Technol.* 3 (3) (2018) 030502.
- [18] Samuel Yen-Chi Chen, Yoo Shinjae, Yao-Lung L. Fang, Quantum long short-term memory, in: ICASSP 2022-2022 IEEE International Conference on Acoustics, Speech and Signal Processing, ICASSP, IEEE, 2022.
- [19] A. Mari, T.R. Bromley, J. Izaac, M. Schuld, N. Killoran, Transfer learning in hybrid classical-quantum neural networks, *Quantum* 4 (2020) 340.
- [20] K. He, X. Zhang, S. Ren, J. Sun, Deep residual learning for image recognition, in: Proceedings of the IEEE Conference on Computer Vision and Pattern Recognition, 2016.
- [21] A. Krizhevsky, G. Hinton, Learning multiple layers of features from tiny images, 7, 2009.
- [22] E.H. Houssein, Z. Abobashima, M. Elhoseny, W.M. Mohamed, Hybrid quantum-classical convolutional neural network model for COVID-19 prediction using chest X-ray images, *J. Comput. Des. Eng.* 9 (2) (2022) 343–363.
- [23] M.A. Nielsen, I. Chuang, *Quantum computation and quantum information*, 2002.
- [24] Edward Farhi, Hartmut Neven, Classification with quantum neural networks on near term processors, 2020, arXiv preprint [arXiv:1802.06002](https://arxiv.org/abs/1802.06002).
- [25] I.D. Apostopoulos, T.A. Mpesiana, Covid-19: automatic detection from x-ray images utilizing transfer learning with convolutional neural networks, *Phys. Eng. Sci. Med.* 43 (2) (2020) 635–640.
- [26] S. Jamil, M. Rahman, A dual-stage vocabulary of features (VoF)-based technique for COVID-19 variants' classification, *Appl. Sci.* 11 (24) (2021) 11902.
- [27] W. Ullah, A. Ullah, K.M. Malik, A.K.J. Saudagar, M.B. Khan, M.H.A. Hasanat, A. Altameem, M. Alkhathami, Multi-stage temporal convolution network for COVID-19 variant classification, *Diagnostics* 12 (11) (2022) 2736.
- [28] S. Showkat, S. Qureshi, Efficacy of transfer learning-based ResNet models in chest X-ray image classification for detecting COVID-19 pneumonia, *Chemometr. Intell. Lab. Syst.* 224 (2022) 104534.
- [29] E. Khan, M.Z.U. Rehman, F. Ahmed, F.A. Alfouzan, N.M. Alzahrani, J. Ahmad, Chest chest X-ray classification for the detection of COVID-19 using deep learning techniques, *Sensors* 22 (3) (2022) 1211.
- [30] Y. Araf, F. Akter, Y.D. Tang, R. Fatemi, M.S.A. Parvez, C. Zheng, M.G. Hossain, Omicron variant of SARS-CoV-2: genomics, transmissibility, and responses to current COVID-19 vaccines, *J. Med. Virol.* 94 (5) (2022) 1825–1832.
- [31] Y. Oh, S. Park, J.C. Ye, Deep learning COVID-19 features on CXR using limited training data sets, *IEEE Trans. Med. Imaging* 39 (8) (2020) 2688–2700.
- [32] Xiangjun Wu, et al., Deep learning-based multi-view fusion model for screening 2019 novel coronavirus pneumonia: a multicentre study, *Eur. J. Radiol.* 128 (2020) 109041.
- [33] J.E. Mooij, T.P. Orlando, L. Leviton, L. Tian, C.H. Van der Wal, S. Lloyd, Josephson persistent-current qubit, *Science* 285 (5430) (1999) 1036–1039.
- [34] M. Zidan, A. Abdel-Aty, A. Younes, E.A. Zanaty, I. El-Khayat, M. Abdel-Aty, A novel algorithm based on entanglement measurement for improving speed of quantum algorithms, *Appl. Math. Inf. Sci.* 12 (1) (2018) 265–269.
- [35] J.A. Jones, M. Mosca, R.H. Hansen, Implementation of a quantum search algorithm on a quantum computer, *Nature* 393 (6683) (1998) 344–346.
- [36] Maria Schuld, Nathan Killoran, Quantum machine learning in feature Hilbert spaces, *Phys. Rev. Lett.* 122 (4) (2019) 040504.
- [37] X. Wu, H. Hui, M. Niu, L. Li, L. Wang, B. He, et al., Deep learning-based multi-view fusion model for screening 2019 novel coronavirus pneumonia: a multicentre study, *Eur. J. Radiol.* 128 (2020) 109041.
- [38] S. Rahman, S. Sarker, M.A.A. Miraj, R.A. Nihal, A.K.M. Nadimul Haque, A.A. Noman, Deep learning-driven automated detection of Covid-19 from radiography images: A comparative analysis, *Cogn. Comput.* (2021) 1–30.
- [39] V. Bergholm, J. Izaac, M. Schuld, C. Gogolin, M.S. Alam, S. Ahmed, et al., PennyLane: Automatic differentiation of hybrid quantum-classical computations, 2018, arXiv preprint [arXiv:1811.04968](https://arxiv.org/abs/1811.04968).
- [40] Tarun Agrawal, Prakash Choudhary, FocusCovid: automated COVID-19 detection using deep learning with chest X-ray images, *Evolv. Syst.* (2021) 1–15.
- [41] N. Ullah, J.A. Khan, S. Almakdi, M.S. Khan, M. Alshehri, D. Alboaneen, A. Raza, A novel CovidDetNet deep learning model for effective COVID-19 infection detection using chest radiograph images, *Appl. Sci.* 12 (12) (2022) 6269.
- [42] N. Ullah, J.A. Khan, S. El-Sappagh, N. El-Rashidy, M.S. Khan, A holistic approach to identify and classify COVID-19 from chest radiographs, ECG, and CT-scan images using ShuffleNet convolutional neural network, *Diagnostics* 13 (1) (2023) 162.
- [43] Y. Sun, L. Guo, T.T. Teoh, A transfer learning method for Covid-19 and pneumonia diagnosis based on chest radiograph classification, in: 2023 15th International Conference on Computer Research and Development, ICCRD, IEEE, 2023, pp. 167–175.
- [44] Essam H. Houssein, Zainab Abobashima, Mohamed Elhoseny, Waleed M. Mohamed, Hybrid quantum-classical convolutional neural network model for COVID-19 prediction using chest X-ray images, *J. Comput. Des. Eng.* 9 (2) (2022) 343–363.